Ultrafast ellipsometry of coherent processes and exciton-exciton interactions in quantum wells at negative delays

J. A. Bolger, A. E. Paul, and Arthur L. Smirl
Laboratory for Photonics and Quantum Electronics, 100 IATL, University of Iowa, Iowa City, Iowa 52242
(Received 18 April 1996)

A combination of ellipsometric and pump-probe techniques are used to completely determine the time-averaged and time-resolved polarization state of the degenerate four-wave-mixing signal emitted from a $GaAs/Al_xGa_{1-x}As$ multiple quantum well following femtosecond excitation for negative time delays between the pump and probe. The polarization state of the four-wave-mixing signal is observed to exhibit a continuously varying ellipticity and a real-time rotation of the polarization ellipse at negative time delays that are dramatically and functionally different from those observed at positive delays. These distinct polarization features place stringent constraints on the physical models and are shown to be consistent with the inclusion of both many-body interactions and biexcitonic effects. [S0163-1829(96)02139-X]

I. INTRODUCTION

One of the techniques that has proven to be extremely powerful for studying coherent processes and excitonic effects in semiconductors and multiple quantum wells (MQW's) is to study the polarization dependence of the degenerate four-wave-mixing (FWM) process.[1–19] To date, such polarization observations have been successfully interpreted in terms of the so-called local-field corrections (LFC),[2,17,20–27] the density-dependent excitation-induced dephasing (EID),[8–10,19,28,29] or biexciton formation (BIF).[30–34] Typically, in these studies, the dependence of the magnitude of the FWM signal (or its spectrum) on the incident polarizations[2–16] has been measured, and there have been very few attempts[17–19] to monitor the polarization state of the emitted FWM signal itself. Moreover, the latter studies[17–19] have been restricted to measurements of the direction of polarization (ignoring the ellipticity and the degree of polarization) and, therefore, they have not completely specified the polarization state of the emitted light.

Recently, however, we have used a procedure that combines standard ellipsometric and time-resolved pump-probe techniques to *completely* determine the polarization state of both the time-integrated (TI-FWM) (Ref. 35) and time-resolved FWM (TR-FWM) (Ref. 36) emission from a $GaAs/Al_xGa_{1-x}As$ MQW. In those studies,[35,36] the FWM signal was shown to be completely polarized at each instant, but both the ellipticity and the orientation of the polarization ellipse varied dramatically and continuously with time during emission. Moreover, the ellipticity and the orientation of the polarization ellipse were each shown to be strongly dependent on the carrier density and the incident polarizations. Most importantly, the polarization states of both the TI-FWM and the TR-FWM were found to exhibit qualitative features that placed additional constraints on models describing FWM in MQW's. By comparing our results to a model based on the optical Bloch equations with LFC, EID, and BIF included phenomenologically, we found[36] that our TI-FWM measurements were not definitive in determining the role of the various processes. That is, the gross features in our TI-FWM polarization data could be reproduced either by including LFC and EID together, by BIF acting alone, or by including all three. By contrast, the qualitative features in our TR-FWM polarization data could be reproduced only by including all three processes. We emphasize, however, that our previous measurements have been restricted to positive delays between the two incident pulses.

In this paper, we describe measurements in which we *completely* determine the polarization state of both the TI-FWM and the TR-FWM emission from a $GaAs/Al_xGa_{1-x}As$ MQW *at negative time delays* (i.e., when the probe arrives before the pump). In contrast to measurements performed at positive delays, one advantage of this configuration is that direct FWM emission from isolated excitons cannot contribute to the signal. Only contributions from LFC, EID, and BIF would be expected to contribute. As for positive delays, we show (i) that the FWM signal is indeed completely polarized at each instant of time, (ii) that both the ellipticity and the orientation of the polarization ellipse vary dramatically and continuously with time during the emission, and (iii) that the polarizations of the TI-FWM and the TR-FWM signals are strongly dependent on the relative polarizations of the linearly polarized input pulses. The qualitative behavior of the polarization state for negative delays, however, is dramatically different from that observed for positive delays. Furthermore, in contrast to the results obtained at positive delays, the time-integrated studies at negative delays are more definitive in determining which processes do or do not contribute to the emitted signal. Nevertheless, we demonstrate that the observed behavior (like that at positive delays) is consistent with the inclusion of both biexcitons and many-body effects.

II. ULTRAFAST ELLIPSOMETRY

The TR-FWM measurements were performed using 160 fs pulses from a tunable mode-locked Ti:sapphire laser and the conventional two-pulse FWM geometry shown in Fig. 1(a). The experimental parameters and procedures are identical to those reported in our previous paper,[36] except that for the measurements described here the time delay between the

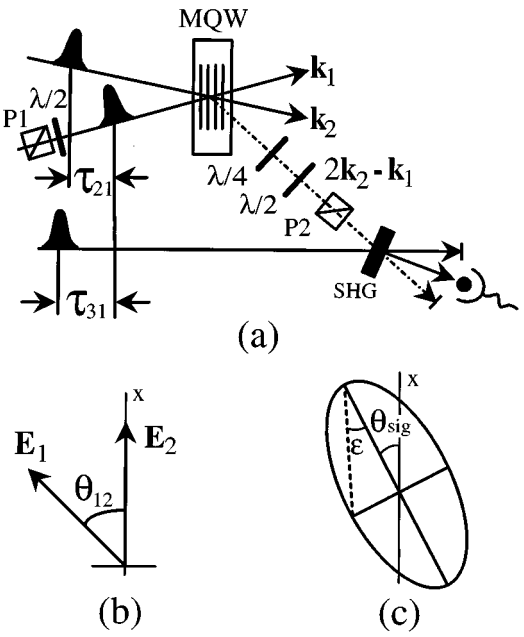

FIG. 1. Schematic of (a) the experimental geometry for time-resolving the polarization state of the emitted FWM signal, where λ/4 denotes a quarter-wave plate, λ/2 a half-wave plate, SHG a second-harmonic generation crystal, and $P1$ and $P2$ represent polarizers; (b) the relative orientations of the linear pump ($\mathbf{E_1}$) and probe ($\mathbf{E_2}$) input polarizations; and (c) the polarization ellipse associated with the emitted FWM signal showing the azimuthal angle θ_{sig} and the ellipticity angle ε.

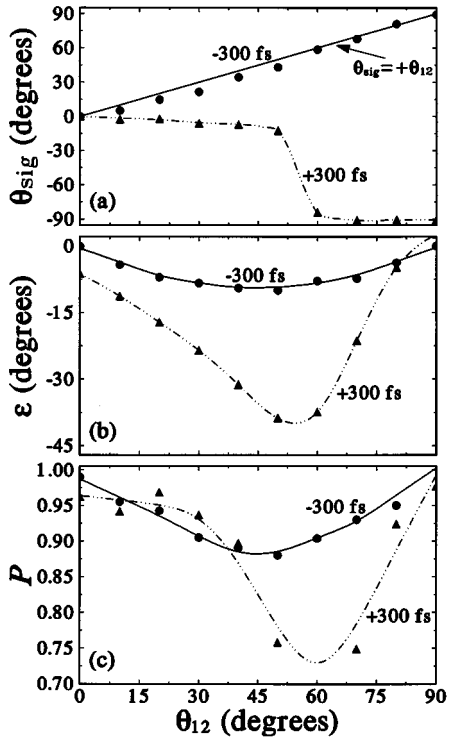

FIG. 2. Measurements of the time-averaged (a) azimuthal angle θ_{sig}, (b) ellipticity angle ε, and (c) the degree of polarization P as a function of the angle θ_{12} between the two input polarizations for a fixed negative delay $\tau_{21}=-300$ fs (solid circles) and for a fixed positive delay $\tau_{21}=+300$ fs (solid triangles) for a total peak fluence of 1.0 μJ/cm^2. The lines are only a guide to the eye.

two pulses τ_{21} ($\equiv t_2-t_1$) was fixed at a negative value of -300 ps (i.e., the probe $\mathbf{E_2}$ arrives before the pump $\mathbf{E_1}$). A quarter-wave plate, a half-wave plate, and an analyzer were used (as described in Ref. 36) to determine the fraction P of the light that was polarized ($P=1$ denotes completely polarized light) and to extract the ellipticity angle ϵ and the azimuthal angle θ_{sig} for the polarization ellipse associated with the polarized portion [see Fig. 1(c)] of the FWM signal. The TR-FWM signal transmitted by these components was measured by cross correlating it with a reference pulse in a second-harmonic generation (SHG) crystal. For the TI-FWM measurements, the SHG crystal was removed and was replaced with a detector which integrated the FWM signal. In this way, the complete polarization states of the TI-FWM and the TR-FWM signals were measured as a function of the angle θ_{12} between the two linear input polarizations $\mathbf{E_1}$ and $\mathbf{E_2}$ [see Fig. 1(b)].

The MQW sample used in these measurements is also the same one used in Ref. 36. It consists of 10 periods of 14-nm-wide GaAs wells separated by 17-nm-wide $Al_{0.3}Ga_{0.7}As$ barriers. The sample was processed by mounting it onto a glass flat, by removing the substrate with a selective etch to permit transmission measurements, and by applying an antireflection coating to the exposed semiconductor-air interface to reduce Fabry-Perot effects. The measurements reported here were performed at 80 K. At this temperature, the heavy-hole (hh) exciton is predominantly homogeneously broadened and has a linewidth of 1.3 meV. The splitting between the heavy- and light-hole excitons is 7.3 meV. The laser pulse, which had a bandwidth of 12 meV, was tuned to 6 meV below the hh exciton. As we have discussed previously, with this bandwidth and this detuning, we estimate the initial light-hole exciton and free-carrier populations to be less than 5% of the heavy-hole population. To allow a direct comparison with our previous TR-FWM measurements at the corresponding positive delay of $+300$ fs, we used the same excitation fluence (1 μJ/cm^2) as in those studies.[36] At this fluence, we estimate the heavy-hole areal density to be $\sim 4\times10^9$ cm^{-2} (corresponding to $\sim 3\times10^{15}$ cm^{-3}). Notice that this density is in the low to moderately low regime as defined in our initial TI-FWM studies[35] (and it is more than a factor of 5 below the high-density regime). This was the smallest excitation level for which we could maintain a robust signal-to-noise ratio for a MQW of this thickness at this temperature using this technique.

III. POLARIZATION STATE OF THE FWM SIGNAL AT NEGATIVE DELAYS

Typical time-integrated results at a negative time delay of -300 fs are summarized in Fig. 2 (solid circles) for selected angles between the two input polarizations and for an excitation fluence of ~ 1 μJ/cm^2. Notice that the time-averaged polarization associated with the TI-FWM signal has a significant unpolarized component and that the polarized portion is elliptically polarized. In addition, the degree of polarization, the ellipticity, and the orientation of the polarization ellipse are each strongly dependent on the relative orienta-

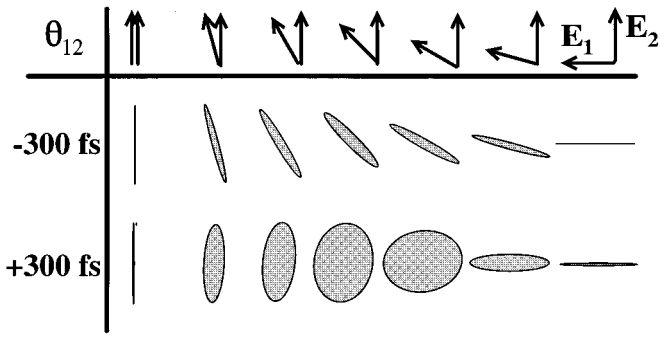

FIG. 3. Sketches of the polarization ellipses corresponding to the data in Fig. 2.

tions of the incident linear polarizations. The time-integrated behavior shown in Fig. 2 is, however, significantly different from that observed at positive delays.[36] To emphasize these dramatic differences, we have also plotted the corresponding data (solid triangles) for a positive delay of the same magnitude (+300 fs) taken from our previous paper.[36] In addition, in Fig. 3, we have sketched the polarization ellipses corresponding to the data of Fig. 2. Several differences between positive and negative delay are worth noting. Most importantly, the direction of rotation of the major axis of the polarization ellipse (θ_{sig}) for positive delays is opposite to that for negative delays. For the negative delay, the azimuthal angle associated with the emitted radiation rotates in the same direction (counterclockwise) as the incident polarization. By contrast, for the positive delay, the ellipse rotates clockwise as the input polarization rotates counterclockwise. In addition, for the negative delay, the counterclockwise rotation is smooth and continuous (i.e., $\theta_{sig} \sim +\theta_{12}$), while for the positive delay, a sudden jump in the clockwise rotation from small negative angles to negative angles near $-90°$ is observed for $\theta_{12} \sim 50°$. Finally, the ellipticity and the fraction of unpolarized light are both significantly smaller for the negative delay.

The corresponding time-resolved measurements are shown in Fig. 4, where again we have included the results for a positive delay $\tau_{12} = +300$ fs for direct comparison.[36] The data in Fig. 4(a) and 4(b) show that the TR-FWM signal at -300 fs is completely polarized at each instant of time ($P \sim 1$), but that both the ellipticity and the orientation of the polarization ellipse vary continuously with time during the emission. We also find that the temporal behavior of the TR-FWM polarization is strongly dependent on the relative polarizations of the linearly polarized input pulses. Numerical integration of the time-resolved Stokes parameters (not shown) demonstrates that the TR-FWM polarization measurements (Fig. 4) are consistent with the TI-FWM polarization measurements (Fig. 2). The latter verifies that the unpolarized fraction of the TI-FWM signal [Fig. 2(c)] is the result of integrating a continuously time-varying (but deterministic) polarization over the FWM emission time. Again, most importantly, notice that the functional dependence of the polarization ellipse (θ_{sig} and ϵ) on time for the negative delay is different than it is for positive delays. Specifically, notice that for the negative delay, the ellipse [Fig. 4(a)] always rotates clockwise with increasing time. By comparison, for the same positive delay, a distinct bifurcation in the temporal evolution of the azimuthal angle is observed [Fig. 4(c)]. Specifically, for small counterclockwise rotations of θ_{12}, the ellipse is observed to rotate counterclockwise (toward more positive angles) with increasing time, but for larger angles, the ellipse reverses direction and rotates clockwise. Also notice that the magnitude of the ellipticity ϵ of the FWM signal tends to monotonically decrease with time at the negative delay (for a fixed θ_{12} between the two input polarizations), while it is observed to increase then decrease at the positive delay.

IV. COMPARISON WITH THEORY

Both the time-integrated and the time-resolved dynamics of the polarization of the FWM signal at negative delays exhibit qualitative features that place additional constraints on models describing FWM in MQW's. In this section, we

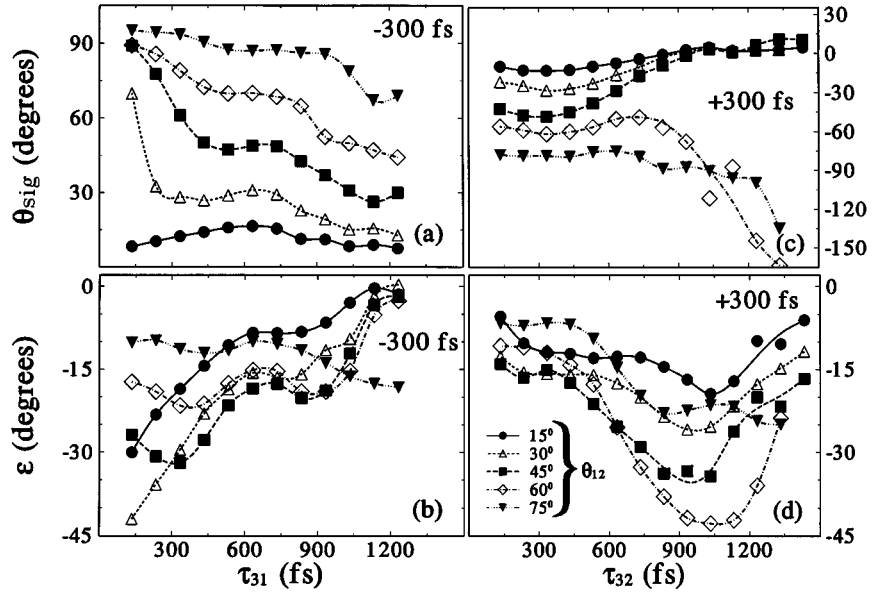

FIG. 4. Time-resolved measurements of the azimuthal angle θ_{sig} and the ellipticity angle ε as a function of time for selected angles θ_{12} between the two input polarizations, for a total peak fluence of 1.0 μJ/cm^2, and for a fixed negative delay $\tau_{21} = -300$ fs and for a fixed positive delay $\tau_{21} = +300$ fs. The lines only connect data points as a rough guide to the eye.

will illustrate these constraints by comparing our results to a model based on the optical Bloch equations with local-field corrections, excitation-induced dephasing, and biexciton formation included phenomenologically. The model is the same as the one used to describe our measurements at positive delays and a more detailed discussion of the model can be found in Ref. 36. In addition, a recent discussion of the connection between the phenomenological approach taken here and a more rigorous approach based on the Semiconductor Bloch Equation formalism can be found in Ref. 37.

Even though we have chosen the parameters in this model to be consistent with our experimental conditions, not all values are precisely known. Consequently, as in our previous paper,[36] we will not rely on quantitative agreement in making our comparisons between theory and experiment, but we will look for qualitative features that are insensitive to fit parameters to identify the contributions of the various processes. In so doing, we will demonstrate that the same combination of processes that produced agreement with the gross features in the data at positive delays also produces agreement with the qualitative features at negative delays.

We emphasize that for purposes of producing the simulations shown in this paper we have used the same numerical values for all parameters as were used in our previous paper at positive delays.[36] Specifically, we have taken the biexciton binding energy to be 1.5 meV. We also have assumed the dephasing rates for the biexciton-to-exciton γ_b^{-1} and the biexciton-to-ground γ_{bg}^{-1} transitions are equal (720 fs) and are roughly the same as the dephasing rate for the exciton γ^{-1} (1 ps). In addition, the LFC parameter and the EID parameter were set to $\xi=0.7$ meV (or 0) and $\eta=2$ meV (or 0), respectively, depending on whether these processes were turned on (or off). Finally, we have assumed that the matrix element for the exciton-to-biexciton transition is the same as that for the exciton to ground-state transition.

The additional constraints placed on the physical model by the negative delay data are illustrated by the numerical results shown in Fig. 5. This figure summarizes and illustrates the qualitative tendencies for the time-averaged azimuthal angle θ_{sig}, the ellipticity ε, and the degree of polarization P at -300 fs when (i) LFC and EID are included in the model, but BIF is not, (ii) BIF acts alone, and (iii) all three processes act in concert. These combinations were chosen for comparison because each produced qualitative agreement with the TI-FWM polarization data at a positive delay of $+300$ fs.[35,36]

At a negative delay of -300 fs, however, the inclusion of both EID and LFC produces elliptically polarized light, in qualitative agreement with the data, but a knee is produced in the azimuthal angle, and the ellipse rotates clockwise—both in disagreement with the data [see Fig. 2(a) and 2(b)]. Moreover, the TI-FWM signal at -300 fs has no time-averaged unpolarized component ($P=1$), which is also contrary to our observations [Fig. 2(c)]. Consequently, LFC and EID acting together will not reproduce the required features at negative delays. By comparison, BIF acting alone produces a smooth rotation in the counterclockwise direction, as required by the data, but the FWM signal is completely ($P=1$) and linearly polarized ($\varepsilon=0^0$), which is not consistent with the observed tendencies. Thus, BIF acting alone cannot account for the time-integrated observations at negative delays.

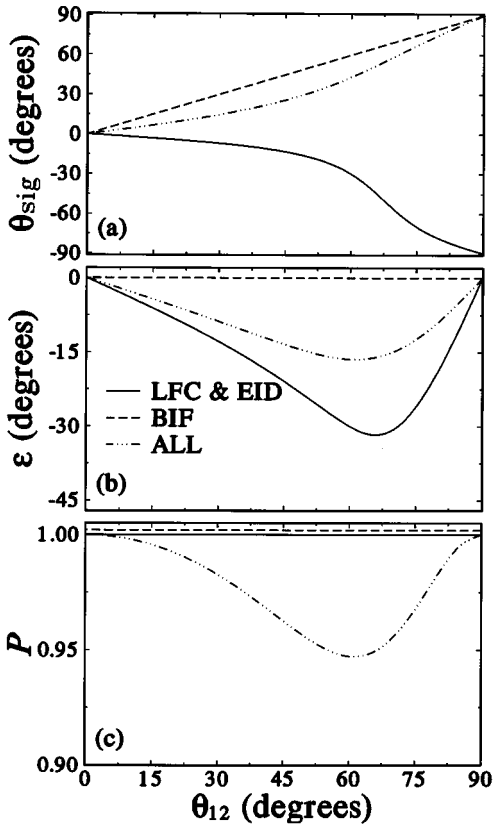

FIG. 5. Comparison of the calculated values at a negative delay of $\tau_{21}=-300$ fs for the time-averaged (a) azimuthal angle θ_{sig}, (b) ellipticity angle ε, and (c) the degree of polarization P as a function of the angle θ_{12} between the two input polarizations for the cases in which both LFC and EID are included, but BIF is excluded (solid line); BIF is included, but LFC and EID are excluded (dashed line); LFC, EID, and BIF are all included (dot dot dot dashed line).

As shown in Fig. 5, however, a model that includes all three processes (BIF, LFC, and EID) will produce the essential features needed for agreement with the time-integrated Stokes measurements at negative delays. Namely, a smooth rotation in the counterclockwise direction is predicted, along with a small, but definite, ellipticity and a time-averaged unpolarized component. From this example, it is clear that the time-averaged ellipsometric measurements at a negative delay place additional constraints on the model describing the FWM process. These constraints eliminate two possibilities that were not excluded by similar measurements at positive delays.

The time-resolved measurements of the state of polarization of the FWM signal as displayed in Fig. 4 obviously place further constraints on the modeling. We have shown previously[36] that when all three processes are included, the major features observed in the TR-FWM polarization data at $\tau_{21}=+300$ fs [and reproduced in Fig. 4(c) and 4(d)] are also present in the numerical simulations. Specifically, at positive delays, we have shown that the calculated ellipticity increases then decreases with time and, most importantly, that the calculated azimuthal angle exhibits a distinct bifurcation in time. That is, the polarization ellipse rotates toward more

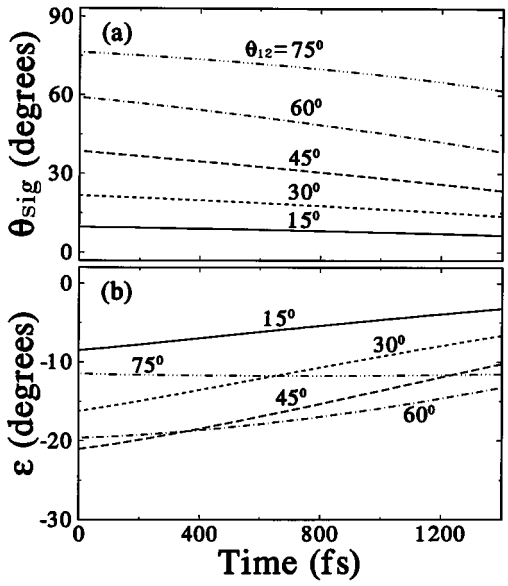

FIG. 6. Calculated values at a negative delay of $\tau_{21}=-300$ fs for the (a) azimuthal angle θ_{sig} and (b) ellipticity angle ε as a function of time for selected angles θ_{12} between the two input polarizations when all three processes, LFC, EID, and BIF, are included.

positive angles for small θ_{12} and toward more negative angles for large θ_{12}. The simulations shown in Fig. 6 illustrate that the same model also produces acceptable agreement with the principal tendencies in the time-resolved data at a negative delay of $\tau_{21}=-300$ fs. Notice that in this case (in agreement with the data), rotation is always in the clockwise direction and no bifurcation is observed. Also, notice that the magnitude of the ellipticity gently, but monotonically, decreases (or stays the same), rather than increasing then decreasing as it does at positive delays. Finally, the magnitude of the ellipticity has roughly the correct ordering with increasing θ_{12}.

V. SUMMARY

Here, we have presented both time-integrated and time-resolved ellipsometric measurements that completely determine the polarization state of the coherently scattered FWM signal from a semiconductor multiple quantum well for a *negative time delay* between the pump and probe. These results indicate that the polarization state of the FWM signal is, in general, elliptical, that the degree of ellipticity varies in time during the emission, and that the orientation of the ellipse continuously rotates in time. We have contrasted our results at negative delays with those that we obtained earlier in the same sample at positive delays,[35,36] and we find that the polarization states associated with both the TI-FWM and TR-FWM signals behave dramatically differently at negative delays than at positive delays. For example, we have found that, as we rotate the linear polarization of the pump counterclockwise through an angle θ_{12} with respect to the stationary linear polarization of the probe, the orientation of the polarization ellipse associated with the TI-FWM signal rotates counterclockwise for negative delays and clockwise for positive delays. In addition, the functional dependencies of the ellipticity and the orientation of the polarization ellipse on time and on incident polarization directions were dramatically different for negative and positive delays. These measurements place additional and more stringent constraints on any successful model of the physical processes responsible for the FWM in semiconductor MQW's. Nevertheless, we have shown that all of the qualitative features associated with the measurements at negative delays can be reproduced by the same phenomenological model that we have used to account for our results at positive delays.

ACKNOWLEDGMENTS

This work was supported in part by the Office of Naval Research, the National Science Foundation, and the National Institute for Standards and Technology.

[1] *Coherent Optical Interactions in Semiconductors*, edited by R. T. Phillips (Plenum, New York, 1994), and references therein.
[2] D. S. Kim, J. Shah, T. C. Damen, W. Schäfer, F. Jahnke, S. Schmitt-Rink, and K. Köhler, Phys. Rev. Lett. **69**, 2725 (1992).
[3] S. T. Cundiff, H. Wang, and D. G. Steel, Phys. Rev. B **46**, 7248 (1992).
[4] S. Schmitt-Rink, D. Bennhardt, V. Heuckeroth, P. Thomas, P. Haring, G. Maidorn, H. Bakker, K. Leo, D. S. Kim, J. Shah, and K. Kohler, Phys. Rev. B **46**, 10 460 (1992).
[5] S. T. Cundiff and D. G. Steel, IEEE J. Quantum Electron. **QE-28**, 2423 (1992).
[6] D. Bennhardt, P. Thomas, R. Eccleston, E. J. Mayer, and J. Kuhl, Phys. Rev. B **47**, 13 485 (1993).
[7] H. H. Yaffe, Y. Prior, J. P. Harbison, and L. T. Florez, J. Opt. Soc. Am. B **10**, 578 (1993).
[8] H. Wang, K. Ferrio, D. G. Steel, Y. Z. Hu, R. Binder, and S. W. Koch, Phys. Rev. Lett. **71**, 1261 (1993).
[9] T. Rappen, U. G. Peter, M. Wegener, and W. Schäfer, Phys. Rev. B **49**, 10 774 (1994).
[10] D. G. Steel, H. Wang, M. Jiang, K. Ferrio, and S. T. Cundiff, in *Coherent Optical Interactions in Semiconductors*, edited by R. T. Phillips (Plenum, New York, 1994), p. 157.
[11] H. Wang, J. Shah, T. C. Damen, and L. N. Pfeiffer, Solid State Commun. **91**, 869 (1994).
[12] T. Saiki, M. Kuwata-Gonokami, T. Matsusue, and H. Sakaki, Phys. Rev. B **49**, 7817 (1994).
[13] D. S. Kim, J. Shah, T. C. Damen, L. N. Pfeiffer, and W. Schäfer, Phys. Rev. B **50**, 5775 (1994).
[14] E. J. Mayer, G. O. Smith, V. Heuckeroth, J. Kuhl, K. Bott, A. Schulze, T. Meier, D. Bennhardt, S. W. Koch, P. Thomas, R. Hey, and K. Ploog, Phys. Rev. B **50**, 14 730 (1994).
[15] H. Schneider and K. Ploog, Phys. Rev. B **49**, 17 050 (1994).
[16] E. J. Mayer, G. O. Smith, V. Heuckeroth, J. Kuhl, K. Bott, A. Schulze, T. Meier, S. W. Koch, P. Thomas, R. Hey, and K. Ploog, Phys. Rev. B **51**, 10 909 (1995).
[17] K. Bott, O. Heller, D. Bennhardt, S. T. Cundiff, P. Thomas, E. J. Mayer, G. O. Smith, R. Eccleston, J. Kuhl, and K. Ploog, Phys. Rev. B **48**, 17 418 (1993).
[18] R. Eccleston, J. Kuhl, D. Bennhardt, and P. Thomas, Solid State Commun. **86**, 93 (1993).

[19] Z. Hu, R. Binder, S. W. Koch, S. T. Cundiff, H. Wang, and D. G. Steel, Phys. Rev. B **49**, 14 382 (1994).
[20] K. Leo, M. Wegner, J. Shah, D. S. Chemla, E. O. Göbel, T. C. Damen, S. Schmitt-Rink, and W. Schäfer, Phys. Rev. Lett. **65**, 1340 (1990).
[21] M. Wegener, D. S. Chemla, S. Schmitt-Rink, and W. Schäfer, Phys. Rev. A **42**, 5675 (1990).
[22] K. Leo, Appl. Phys. A **53**, 118 (1991).
[23] K. Leo, E. O. Göbel, T. C. Damen, J. Shah, S. Schmitt-Rink, W. Schäfer, J. F. Müller, K. Köhler, and P. Ganser, Phys. Rev. B **44**, 5726 (1991).
[24] S. Schmitt-Rink, S. Mukamel, K. Leo, J. Shah, and D. S. Chemla, Phys. Rev. A **44**, 2124 (1991).
[25] S. Weiss, M.-A. Mycek, J.-Y. Bigot, S. Schmitt-Rink, and D. S. Chemla, Phys. Rev. Lett. **69**, 2685 (1992).
[26] J.-Y. Bigot, M.-A. Mycek, S. Weiss, R. G. Ulbrich, and D. S. Chemla, Phys. Rev. Lett. **70**, 3307 (1993).
[27] W. Schäfer, F. Jahnke, and S. Schmitt-Rink, Phys. Rev. B **47**, 1217 (1993).
[28] L. Schultheis, J. Kuhl, A. Honold, and C. W. Tu, Phys. Rev. Lett. **57**, 1635 (1986).
[29] A. Honold, L. Schultheis, J. Kuhl, and C. W. Tu, Phys. Rev. B **40**, 6442 (1989).
[30] B. F. Feuerbacher, J. Kuhl, and K. Ploog, Phys. Rev. B **43**, 2439 (1991).
[31] R. Raj, I. Abram, and J. A. Levenson, Solid State Commun. **81**, 51 (1992).
[32] S. Bar-Ad and I. Bar-Joseph, Phys. Rev. Lett. **68**, 349 (1992).
[33] D. J. Lovering, R. T. Phillips, G. J. Denton, and G. W. Smith, Phys. Rev. Lett. **68**, 1880 (1992).
[34] K.-H. Pantke, D. Oberhauser, V. G. Lyssenko, J. M. Hvam, and G. Weimann, Phys. Rev. B **47**, 2413 (1993).
[35] S. Patkar, A. E. Paul, W. Sha, J. A. Bolger, and A. L. Smirl, Phys. Rev. B **51**, 10 789 (1995).
[36] A. E. Paul, J. A. Bolger, and Arthur L. Smirl, J. Opt. Soc. Am. B **13**, 1016 (1996).
[37] K. Victor, V. M. Axt, G. Bartels, A. Stahl, K. Bott, and P. Thomas, Z. Phys. B **99**, 197 (1996).